ASTROPHYSICS

Atom-interferometry constraints on dark energy

P. Hamilton,[1]* M. Jaffe,[1] P. Haslinger,[1] Q. Simmons,[1] H. Müller,[1,2]† J. Khoury[3]

If dark energy, which drives the accelerated expansion of the universe, consists of a light scalar field, it might be detectable as a "fifth force" between normal-matter objects, in potential conflict with precision tests of gravity. Chameleon fields and other theories with screening mechanisms, however, can evade these tests by suppressing the forces in regions of high density, such as the laboratory. Using a cesium matter-wave interferometer near a spherical mass in an ultrahigh-vacuum chamber, we reduced the screening mechanism by probing the field with individual atoms rather than with bulk matter. We thereby constrained a wide class of dark energy theories, including a range of chameleon and other theories that reproduce the observed cosmic acceleration.

Cosmological observations have firmly established that the universe is expanding at an accelerating pace, which can be explained by dark energy permeating all of space and accounting for ~70% of the energy density of the universe (*1*). What constitutes dark energy, and why it has its particular density, remain as some of the most pressing open questions in physics. What is clear is that dark energy presents us with a new energy scale, on the order of milli–electron volts. It is reasonable to speculate that new (usually scalar) fields might be associated with this scale and that these may make up all or part of the dark energy density (*2*, *3*). String theory with "compactified" extra dimensions, for instance, features a plethora of scalar fields, which typically couple directly to matter fields unless protected by a shift symmetry, as for axions (*4*, *5*). If the fields are light, this coupling would be observable as a "fifth force," in potential conflict with precision tests of gravity (*6*).

Theories with so-called screening mechanisms, on the other hand, have features that suppress their effects in regions of high density, so that they may couple to matter but nonetheless evade experimental constraints (*7*). One prominent example is the chameleon field, the mass of which depends on the ambient matter density (*8*, *9*). It is light and mediates a long-range force in sparse environments, such as the cosmos, but it becomes massive and thus short-ranged in a high-density environment, such as the laboratory (fig. S1). This makes it difficult to detect with fifth-force experiments.

Burrage and co-workers (*10*) recently proposed using atom interferometers (*11*, *12*) to search for chameleons. An ultrahigh-vacuum chamber containing atomic test particles simulates the low-density conditions of empty space, liberating the chameleon field to become long-ranged and thus measurable. In this study, we used a cavity-based atom interferometer (*13*, *14*), measuring the force between cesium-133 atoms and an aluminum sphere to search for a range of screened dark energy theories that can reproduce the estimated cosmological dark energy density (Fig. 1, A and B).

The chameleon dark energy field ϕ in equilibrium is determined by minimizing a potential density $V(\phi) + V_{\rm int}$, which is the sum of a self-interaction term $V(\phi)$ and a term $V_{\rm int}$ describing the interaction with ordinary matter. The simplest chameleon theories are characterized by two parameters that have the dimension of mass. The first one, Λ, enters the self-interaction potential term (*15*, *16*)

$$V(\phi) = \Lambda^4 e^{\Lambda^n/\phi^n} \simeq \Lambda^4 + \frac{\Lambda^{4+n}}{\phi^n} + \ldots \quad (1)$$

The term proportional to $1/\phi^n$, where n is a real exponent often taken to be 1, leads to screening, whereas the constant term is responsible for the chameleon's energy density in otherwise empty space. It can drive the cosmic acceleration observed today if $\Lambda = \Lambda_0 \approx 2.4$ meV, given by the current dark energy density of 7×10^{-27} kg/m^3, which is roughly the mass of four hydrogen atoms per cubic meter. The second parameter, M, enters the term for interaction with ordinary matter of density ρ (again using natural units)

$$V_{\rm int} = \frac{\phi\rho}{M} \quad (2)$$

The parameter M is essentially unconstrained but plausibly below the reduced Planck mass $M_{\rm Pl} = (\hbar c/8\pi G)^{1/2} \approx 2.4\times10^{18}$ GeV/c^2. A lower bound, $M > 10^4$ GeV/c^2, was derived from hydrogen spectroscopy (*17*).

Existing experimental bounds for $M < M_{\rm Pl}$ come from oscillations of rubidium atoms in a harmonic trap (*18*) and from ultracold neutrons (*19*, *20*). Limits from astrophysical observations (*7*) and torsion balances (*6*, *21*) are available for $M \approx M_{\rm Pl}$, where the chameleon is unscreened. Experiments such as the Chameleon Afterglow Search [CHASE (*22*)], the Axion Dark Matter Experiment [ADMX (*23*)], and the CERN Axion Solar Telescope [CAST (*24*)] place bounds, given an additional coupling of the chameleon to the photon. Our limits do not depend on such extra couplings.

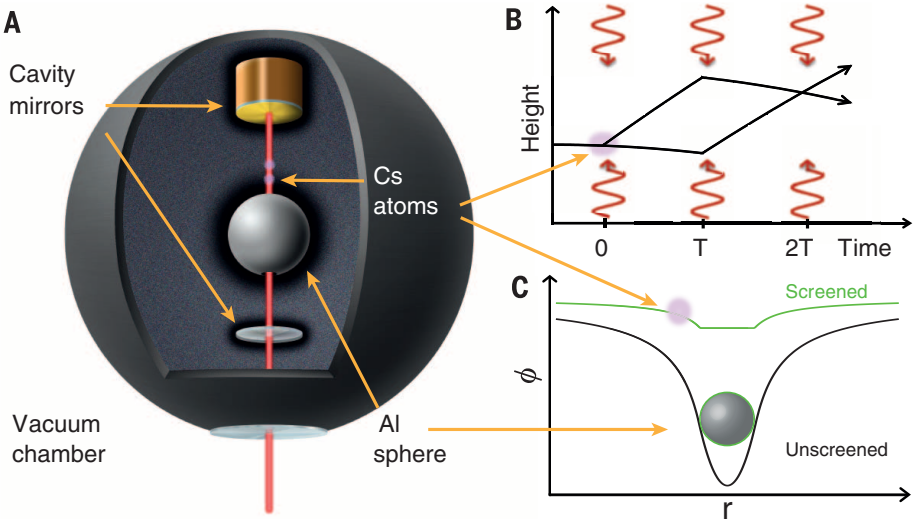

Fig. 1. Screened fields in our experiment. (**A**) The vacuum chamber (radius, 5 cm; pressure, ~6 × 10^{-10} Torr; mostly hydrogen) holds a pair of mirrors forming a Fabry-Perot cavity and the aluminum source sphere. Laser beams pass through a 1.5-mm-radius hole in the sphere (radius of the sphere, 9.5 mm). A Mach-Zehnder interferometer is formed using cold cesium atoms from a magneto-optical trap at an effective distance of 8.8 mm from the sphere surface (not shown). (**B**) Photons in three flashes of laser radiation that are resonant in the cavity impart momentum to the atoms, directing each atomic matter wave onto two paths. (**C**) The potential generated by a macroscopic sphere as a function of distance from the sphere's center.

[1]Department of Physics, 366 Le Conte Hall MS 7300, University of California–Berkeley, Berkeley, CA 94720, USA. [2]Lawrence Berkeley National Laboratory, One Cyclotron Road, Berkeley, CA 94720, USA. [3]Center for Particle Cosmology, Department of Physics and Astronomy, University of Pennsylvania, Philadelphia, PA 19104, USA. *Present address: Department of Physics and Astronomy, 475 Portola Plaza, University of California–Los Angeles, CA 90095, USA. †Corresponding author. E-mail: hm@berkeley.edu

The acceleration of an atom at a radius r from the center of the sphere (Fig. 1A), caused by the sphere via the chameleon interaction and gravity, is given by

$$a \approx \frac{Gm_s}{r^2}\left[1 + 2\lambda_a\lambda_s\left(\frac{M_{Pl}}{M}\right)^2\right] \quad (3)$$

where G is the gravitational constant, and m_s is the mass of the sphere (*10*). The screening factors λ_a and λ_s for the atom and the sphere, respectively, are functions of the object's mass and radius as well as of the parameters Λ, M, and n (eq. S1). They approach 1 for small and light particles. For macroscopic objects, however, only a thin outermost layer will interact with the chameleon field (Fig. 1C), leading to a screening factor much smaller than 1. Macroscopic fifth-force experiments are faced with two small screening factors, but atom interferometers avoid this double suppression.

The operation of the atom interferometer is based on the matter-wave concept of quantum mechanics. When the atom absorbs or emits a photon, it recoils with the momentum $\hbar k$ (where $\hbar$ is the reduced Planck constant, and k is the wavenumber of the photon). We use a two-photon Raman transition between the two hyperfine levels of the ground state of cesium, which are labeled by their total angular momentum quantum numbers of $F = 3$ and 4, respectively. The transition is driven by two vertical, counter-propagating laser beams (Fig. 1A). The atom absorbs a photon from the first beam and is stimulated by the second beam to emit a photon in the opposite direction. The net effect on the atom is a change of the internal quantum state from $F = 3$ to $F = 4$ and an impulse of $\hbar k_{eff}$, where the effective wavenumber k_{eff} is the sum of the wavenumbers of the two beams. The duration and intensity of the laser pulses can be tuned so that the transfer happens with 50 or nearly 100% probability, forming beam splitters and mirrors, respectively, for matter waves.

Our Mach-Zehnder interferometer (Fig. 1B) uses a sequence of three light pulses separated by equal time intervals T. The first pulse splits the matter-wave packet describing each atom into two partial ones that separate with a recoil velocity of about 7 mm/s. The second pulse acts as a mirror that reverses the direction of the relative motion, and the third pulse is a beam splitter that overlaps the partial wave packets. Interference of the partial matter waves determines the probability P that the atoms will arrive in each of the two interferometer outputs

$$P = \cos^2(\Delta\phi/2) \quad (4)$$

where the phase difference accumulated between the partial wave packets (*11*)

$$\Delta\phi = k_{eff}\, a_{tot}\, T^2 \quad (5)$$

is a function of the total acceleration ($a_{tot} = a + g$) of the atoms, the sum of the acceleration due to chameleon-mediated interactions with the sphere (Eq. 3), and the far larger acceleration g due to Earth's gravity (and small systematic effects).

The most sensitive atom interferometers use pulse separation times $T \approx 1$ s, over which the atoms fall up to ~10 m in tall atomic fountains (*25*–*27*). We, however, had to keep the atoms within a few millimeters of the sphere to sample the highest chameleon field gradient, and we were thus constrained to $T \approx 10$ ms, resulting in a 10,000-fold signal reduction. Our cavity-based atom interferometer (*12*, *28*), however, reached relatively high resolution under these constraints.

A full experimental run takes 1.7 s. We prepared about 10 million cesium atoms at a temperature

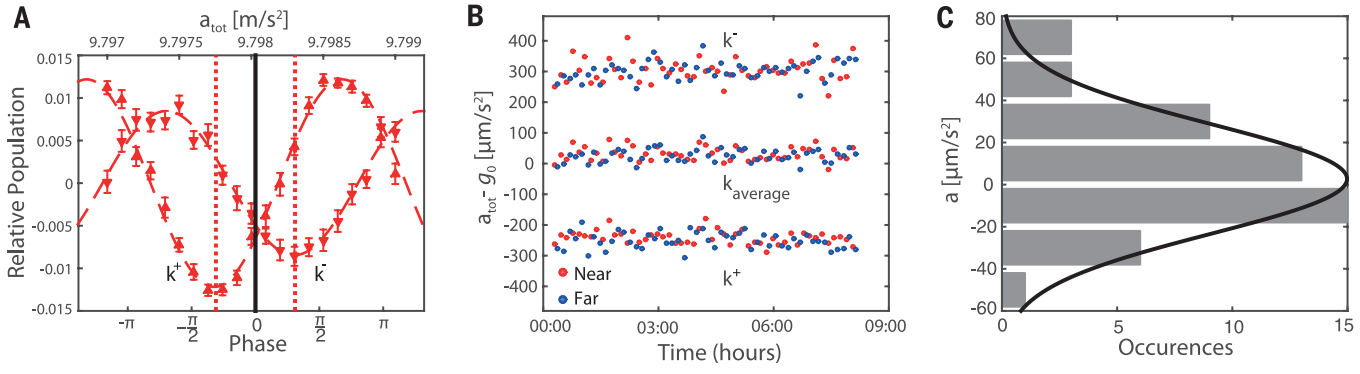

Fig. 2. Data. (**A**) Two interference fringes, measured with the wavevector normal (up, k^+) and inverted (k^-). (**B**) Acceleration $a_{tot} - g_0$, where $g_0 = 9.798$ m/s^2, measured with the wavevector normal and inverted and with the sphere in near (red) and far (blue) positions. The plotted data are from a total of 16,800 runs. Taking the average ($k_{average}$) suppresses systematic effects. Data recorded during the night, before about 6:30 AM, show the lowest noise, suggesting that sensitivity is limited by vibrations. (**C**) Histogram of differences between subsequent measurements with the sphere in the near and far positions.

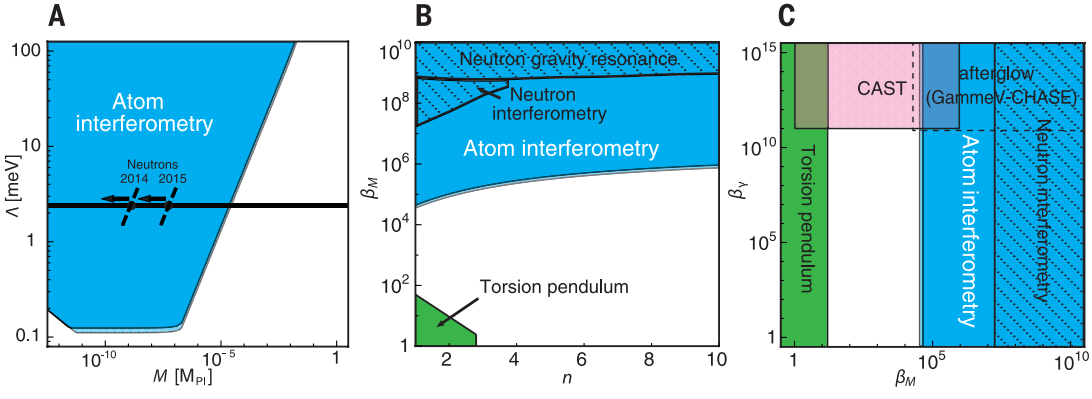

Fig. 3. Regions of exclusion. Blue areas are ruled out by our experiment. The narrow light blue stripes at their borders show the influence of the variation of $0.55 \le \xi \le 0.68$, which arises from different models for the boundary of the vacuum chamber (*14*), demonstrating the robustness of our limits. (**A**) The region excluded at the 95% confidence level in the M-Λ plane for $n = 1$ in Eq. 1. The horizontal line marks the range around $\Lambda_0 = 2.4$ meV, where the chameleon field would reproduce the current cosmic acceleration. Also indicated are the highest values of M excluded by neutron experiments (*19*, *20*); the regions to the left (indicated by arrows) are excluded. (**B**) Comparison of our atom-interferometry results with neutron gravity resonance (*19*) and neutron interferometry (*20*) results in the n-β_M plane, where $\beta_M = M_{Pl}/M$, assuming $\Lambda = \Lambda_0$. Our results are significantly lower for all values of the exponent n and β_M. Torsion pendulum experiments (*6*, *21*) limit chameleons from the other (low-β_M) end of the plane. (**C**) Comparison with CHASE (*22*) and CAST (*24*) experiments that assume photon coupling, assuming $n = 1$ and $\Lambda = \Lambda_0$. Atom interferometers as well as neutron and torsion pendulum experiments give bounds that are independent of the photon coupling parameter β_γ.

of 5 μK in the $F = 3$ state, using a two-dimensional magneto-optical trap (2D-MOT) to load a 3D-MOT through a differential pumping stage. We ran the interferometer with a pulse separation time of $T = 15.5$ ms and identified the two outputs separately via fluorescence detection with a camera (*14*).

Figure 2A shows an interference fringe obtained by measuring the atom number at the two interferometer outputs while varying the phase $\Delta\phi$ (*13*, *14*). Fitting the fringe with a sine wave determines the total acceleration of the atoms. To take out systematic effects, we applied wavevector reversal (i.e., we changed the direction of the photon impulse). This inverts the signal produced by accelerations, but many systematic effects remain unchanged and can be taken out (*29*). To measure the acceleration a originating from atom-sphere interactions (our signal for chameleons) separately from Earth's gravitational acceleration g, we compared the total acceleration $a_{tot} = a + g$ with the sphere located in the "near" position with g measured with the sphere in the "far" position. "Near" means an effective vertical distance of 8.8 mm from the surface of the sphere, and "far" means about 3 cm to the side.

One measurement consists of four interference fringes: two with the wavevector normal (one each with the sphere near and far) and two with the wavevector inverted (as above). Fifty such measurements with their statistical error bars are shown in Fig. 2B. For each, we averaged the acceleration as measured with normal and inverted wavevectors to eliminate systematic effects, and we compared the acceleration thus measured between the near and far positions of the sphere. Figure 2C shows a histogram of these acceleration differences. Fitting a Gaussian distribution to the histogram resulted in an estimate of $a = 2.7 \pm 3.3$ μm/s^2. We added corrections for systematic ac Stark shifts, magnetic fields, and electrostatic fields (*13*) (table S1) and arrived at $a = -0.7 \pm 3.7$ μm/s^2. The negative sign indicates acceleration away from the sphere. The 2σ (95%) confidence interval for these data is -8.2 μm/s^2 $< a <$ 6.8 μm/s^2.

A chameleon has a spin of 0 and can therefore only produce attractive forces (assuming universal coupling to matter). A one-tailed test shows $a <$ 5.5 μm/s^2 at the 95% confidence level. Comparison to the expected acceleration (Eqs. S8 to S11) yields the excluded range of parameters Λ and M, shown in Fig. 3A. Our experiments excluded chameleons at the scale of the cosmological constant $\Lambda = \Lambda_0 =$ 2.4 meV for $M < 2.3 \times 10^{-5}\ M_{Pl}$, making the most conservative assumption of $\xi = 0.55$ for a parameter ξ entering Eqs. S9 and S10 that describes the influence of the vacuum chamber walls (*14*). This result rules out chameleons that would reproduce the observed acceleration of the cosmos. To place our result in the context of previous experiments, we assumed that $\Lambda = \Lambda_0$. Figure 3B shows the excluded region for different values of the exponent n, and Fig. 3C shows the excluded region compared with experiments that assume photon-chameleon coupling (our results do not rely on such a coupling). In short, the only chameleon theories that are still viable are the white areas in Fig. 3, A to C, all of which we have narrowed by several orders of magnitude by using atom interferometry.

Our analysis can be generalized to constrain other scalar field theories, such as symmetron, varying-dilaton, and $f(R)$ theories. These theories belong to the same universality class as the chameleon theories, in that their screening effect is triggered by the local scalar field value, as opposed to its spatial derivatives. As a result, their phenomenology is similar to that of the chameleon (*7*).

REFERENCES AND NOTES

1. Planck Collaboration, http://xxx.lanl.gov/abs/1502.01589 (2015).
2. C. Wetterich, *Nucl. Phys. B* **302**, 668–696 (1988).
3. P. J. E. Peebles, B. Ratra, *Astrophys. J.* **325**, L17 (1988).
4. J. A. Frieman, C. T. Hill, A. Stebbins, I. Waga, *Phys. Rev. Lett.* **75**, 2077–2080 (1995).
5. L. J. Hall, Y. Nomura, S. J. Oliver, *Phys. Rev. Lett.* **95**, 141302 (2005).
6. D. J. Kapner *et al.*, *Phys. Rev. Lett.* **98**, 021101 (2007).
7. A. Joyce, B. Jain, J. Khoury, M. Trodden, *Phys. Rep.* **568**, 1–98 (2015).
8. J. Khoury, A. Weltman, *Phys. Rev. Lett.* **93**, 171104 (2004).
9. D. F. Mota, D. J. Shaw, *Phys. Rev. Lett.* **97**, 151102 (2006).
10. C. Burrage, E. J. Copeland, E. A. Hinds, *J. Cosmol. Astropart. Phys.* **2015**, 042 (2015).
11. M. Kasevich, S. Chu, *Phys. Rev. Lett.* **67**, 181–184 (1991).
12. A. D. Cronin, J. Schmiedmayer, D. E. Pritchard, *Rev. Mod. Phys.* **81**, 1051–1129 (2009).
13. P. Hamilton *et al.*, *Phys. Rev. Lett.* **114**, 100405 (2015).
14. See the supplementary materials on *Science* Online.
15. P. Brax, C. van de Bruck, A. C. Davis, J. Khoury, A. Weltman, *Phys. Rev. D Part. Fields Gravit. Cosmol.* **70**, 123518 (2004).
16. I. Zlatev, L. M. Wang, P. J. Steinhardt, *Phys. Rev. Lett.* **82**, 896–899 (1999).
17. P. Brax, C. Burrage, *Phys. Rev. D Part. Fields Gravit. Cosmol.* **83**, 035020 (2011).
18. D. M. Harber, J. M. Obrecht, J. M. McGuirk, E. A. Cornell, *Phys. Rev. A* **72**, 033610 (2005).
19. T. Jenke *et al.*, *Phys. Rev. Lett.* **112**, 151105 (2014).
20. H. Lemmel *et al.*, *Phys. Lett.* **743**, 310–314 (2015).
21. A. Upadhye, *Phys. Rev. D Part. Fields Gravit. Cosmol.* **86**, 102003 (2012).
22. J. H. Steffen *et al.*, *Phys. Rev. Lett.* **105**, 261803 (2010).
23. G. Rybka *et al.*, *Phys. Rev. Lett.* **105**, 051801 (2010).
24. V. Anastassopoulosa *et al.*, *Phys. Lett. B* 10.1016/j.physletb.2015.07.049 (2015); www.sciencedirect.com/science/article/pii/S0370269315005596.
25. G. Rosi, F. Sorrentino, L. Cacciapuoti, M. Prevedelli, G. M. Tino, *Nature* **510**, 518–521 (2014).
26. A. Sugarbaker, S. M. Dickerson, J. M. Hogan, D. M. S. Johnson, M. A. Kasevich, *Phys. Rev. Lett.* **111**, 113002 (2013).
27. G. M. Tino, M. A. Kasevich, Eds., *Atom Interferometry* (Proceedings of the International School of Physics "Enrico Fermi," vol. 188, IOS Press, Amsterdam, 2014).
28. M. A. Hohensee, B. Estey, P. Hamilton, A. Zeilinger, H. Müller, *Phys. Rev. Lett.* **108**, 230404 (2012).
29. J. M. McGuirk, G. T. Foster, J. B. Fixler, M. J. Snadden, M. A. Kasevich, *Phys. Rev. A* **65**, 033608 (2002).

ACKNOWLEDGMENTS

We acknowledge important discussions with D. Budker, C. Burrage, A. Charman, Y. Nomura, S. Perlmutter, S. Rajendran, and P. Steinhardt. This work was supported by the David and Lucile Packard Foundation; a Defense Advanced Research Projects Agency Young Faculty Award (no. N66001-12-1-4232); NSF grant PHY-1404566; and NASA grants NNH13ZTT002N, NNH13ZTT002N, and NNH11ZTT001N. P.Has. thanks the Austrian Science Fund (grant J3680). The work of J.K. is supported by the NSF Faculty Early Career Development Program (award PHY-1145525) and the NASA Astrophysics Theory Program (grant NNX11AI95G).

SUPPLEMENTARY MATERIALS

www.sciencemag.org/content/349/6250/849/suppl/DC1
Supplementary Text
Figs. S1 to S4
Tables S1 to S4
Equations S1 to S11
Reference (*30*)

12 February 2015; accepted 25 June 2015
10.1126/science.aaa8883

ASTROPHYSICS

Exclusion of leptophilic dark matter models using XENON100 electronic recoil data

The XENON Collaboration*†

Laboratory experiments searching for galactic dark matter particles scattering off nuclei have so far not been able to establish a discovery. We use data from the XENON100 experiment to search for dark matter interacting with electrons. With no evidence for a signal above the low background of our experiment, we exclude a variety of representative dark matter models that would induce electronic recoils. For axial-vector couplings to electrons, we exclude cross sections above 6×10^{-35} cm^2 for particle masses of $m_\chi = 2$ GeV/c^2. Independent of the dark matter halo, we exclude leptophilic models as an explanation for the long-standing DAMA/LIBRA signal, such as couplings to electrons through axial-vector interactions at a 4.4σ confidence level, mirror dark matter at 3.6σ, and luminous dark matter at 4.6σ.

Dark matter in the form of weakly interacting massive particles (WIMPs) is typically expected to induce nuclear recoils in a terrestrial detector target (*1*) with an annually modulated rate due to the motion of the Earth around the Sun (*2*, *3*). Although such a modulation has been observed by the DAMA/LIBRA collaboration using sodium iodine (*4*), it is difficult to interpret it as a dark matter signal, given the null results from other experiments (*5*).

*The XENON Collaboration authors and affiliations are listed in the supplementary materials.
†Corresponding authors: M. Cervantes and R. F. Lang; e-mail: mcervant@purdue.edu, rafael@purdue.edu

Atom-interferometry constraints on dark energy

P. Hamilton, M. Jaffe, P. Haslinger, Q. Simmons, H. Müller and J. Khoury

Science **349** (6250), 849-851.
DOI: 10.1126/science.aaa8883

Limiting unknows in the dark side

Our knowledge of the inventory of stuff that makes up our universe amounts to a humbling 5%. The rest consists of either dark energy (~70%) or dark matter (~25%). Using atom interferometry, Hamilton *et al.* describe the results of experiments that controlled for dark energy screening mechanisms in individual atoms, not bulk matter. Aprile *et al.* report on an analysis of data taken with the XENON100 detectors aiming to identify dark matter particles directly by monitoring their rare interaction with ordinary matter. In this setup, a large underground tank of liquid xenon forms a target for weakly interacting m assive particles. These combined results set limits on several types of proposed dark matter and dark energy candidates (see the Perspective by Schmiedmayer and Abele).

Science, this issue p. 849, p. 851; see also p. 786